

Navigation and Control Methods of an Extravehicular Vehicle for Large Spacecraft

*Feng Yu¹⁾ and Zhengyu Wang²⁾

^{1), 2)} *College of Astronautics, NUAU, No.29 Yudao Street, Nanjing, China*

¹⁾ yufeng@nuaa.edu.cn

ABSTRACT

A new extravehicular vehicle is proposed to assist astronauts to inspect the surface of big spacecraft such as space station or shuttle, so as to guarantee safety of space activity. This vehicle is composed of gyros, accelerometers, a line laser triangulation measuring equipment and a propulsion system. The line laser triangulation measuring equipment consists of an infrared laser, a camera and a filter sheet. The orbit coordinate system of the target spacecraft is selected as the navigation coordinate system. By using the acceleration and angular velocity information measured by gyros and accelerometers, the navigation parameters including the attitude, the angular velocity, the position and the velocity are predicted. When the device drifts over the target spacecraft surface, the line laser triangle measuring equipment collects point cloud data including information of target spacecraft shape. And then the point cloud data in a short time period is unified to a same coordinate system by utilizing short-term high precision of prediction. The measured point cloud data are matched with the known shape structure data of target spacecraft, and then the measured attitude and position relative to the navigation coordinate system are calculated. Navigation parameters including gyro drifts and accelerometer drifts are estimated by combining the prediction and measured attitude and position by utilizing a Kalman filter. Finally, propulsion system is triggered to control the vehicle to drift on target surface.

1. INTRODUCTION

Autonomous on-orbit servicing is to carry out repair, refueling, orbit maintenance, re-orbiting, or other operations for a spacecraft by using smart space robots. The aims include extending the life of a malfunctioned satellite, rebuilding a new satellite by recycling useful parts from decommissioned satellites, or fabricating large spacecraft components such as antennas, solar panels and other multifunctional structures. Due to the importance of the autonomous on-orbit servicing, several on-orbit servicing

¹⁾ Associate Professor

²⁾ Graduate Student

projects including on-orbit servicing demonstration experiments and conceptual on-orbit servicing systems have been carried out. For example, DEOS estimated target motion states by taking a number of images in automatic mode. The Front-end Robotics Enabling Near-term Demonstration (FREND) demonstrated a seven degree-of-freedom (DOF) flight robotic arm in a test-bed with a stereo photogrammetric imaging system.

Space station and space shuttle, which are ultra-large spacecraft, can be regarded as a special class of on-orbit servicing targets. With the development of space technology, space station and other large spacecraft in orbit is increasing. Because large spacecraft often run for a long time in orbit and its size is obviously larger than common satellites, micro-meteoroid impact can cause serious damage which will lead to disasters. In February 2003, the space shuttle Columbia on their homeward way disintegrated, post analysis showed that a thermal insulation tile was off the outer layer of the space shuttle. Therefore, the shuttle melted and disintegrated.

Because of the special space environments, astronauts face many difficulties in the on-orbit inspecting surface of large spacecraft. Space manipulator has been applied to the detection of thermal insulation tile damage on the space shuttle in orbit. Space manipulator has the ability of accurate operation and visual recognition, but the space manipulator also has limited scope of action and can't monitor the whole surface of the spacecraft. It is obvious that the space free flight robot has advantages in on-orbit inspection.

NASA developed a series of Autonomous Extravehicular Activity Robotic Cameras (AERCam) which could be used for remote inspections for International Space Station. The AERCam Sprint was tested on STS-87 and flew very slowly at a rate of less than one-quarter of a foot per second. The follow-on autonomous or teleoperated vehicle called the Mini-AERCam is just 190mm in diameter and weighs approximately 4.5kg. These vehicles maintain attitude stability by gyros, and determine the position by utilizing Differential GPS. The possible disadvantages are that the system couldn't be utilized in the scenario without GPS signals and vehicle attitude will drift slowly as gyros will drift over time.

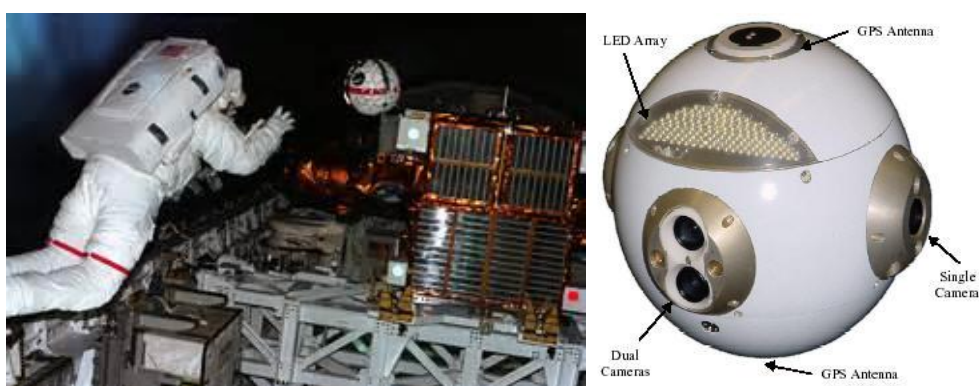


Fig. 1 AERCam Sprint and Mini-AERCam

This paper proposed a new extravehicular vehicle to assistant astronauts to inspect the surface of big spacecraft to guarantee safety of space activity. This vehicle is composed of gyros, accelerometers, a line laser triangulation measuring equipment

and a propulsion system. The line laser triangulation measuring equipment consists of an infrared laser, a camera and a filter sheet. By using the acceleration and angular velocity information measured by gyros and accelerometers, the navigation parameters including the attitude, the angular velocity, the position and the velocity are predicted. When the device drifts over the target spacecraft surface, the line laser triangle measuring equipment collects point cloud data including information of target spacecraft shape. The measured point cloud data are matched with the known shape structure data of target spacecraft, and then the measured attitude and position relative to the navigation coordinate system are calculated. Navigation parameters including gyro drifts and accelerometer drifts are estimated by combining the prediction and measured attitude and position by utilizing a Kalman filter. Finally, an experiment of .line laser triangulation measuring equipment is presented.

2. RELATIVE POSE DETERMINATION PRINCIPLES

There are several major steps to be taken to realize the navigation. The major steps are the prediction of position, velocity and attitude by utilizing acceleration and angular velocity information produced by gyros and accelerometers, integrated navigation and the point cloud data collection from a line laser triangulation measuring equipment.

2.1 Relative pose determination algorithms

The acceleration information of the extravehicular vehicle is determined by accelerometers, and angular velocity information is measured by gyros. The measurements are described as f_c and ω_b respectively. Because accelerometers and gyros include various measurement errors, the measurements are modeled as follows,

$$f_c = f + f_b + f_\varepsilon \quad (1)$$

$$\omega_c = \omega + \omega_b + \omega_\varepsilon \quad (2)$$

where f is acceleration, f_b is accelerometer drift, f_ε is measurement noise which is white noise, ω is angular velocity, ω_b is gyro drift, ω_ε is measurement noise which is regarded as white noise. f_b and ω_b are modeled to be driven by white noise

$$\dot{f}_b = f_{b\varepsilon} \quad (3)$$

$$\dot{\omega}_b = \omega_{b\varepsilon} \quad (4)$$

The linear motion of the extravehicular vehicle relative to the target can be described by Hill equations as

$$\begin{bmatrix} \dot{\rho} \\ \ddot{\rho} \end{bmatrix} = \begin{bmatrix} \mathbf{0}_{3 \times 3} & \mathbf{I}_{3 \times 3} \\ \mathbf{K}(n) & -2[\mathbf{n} \times] \end{bmatrix} \begin{bmatrix} \rho \\ \dot{\rho} \end{bmatrix} + \begin{bmatrix} \mathbf{0}_3 \\ \mathbf{C}_b^o(f_c - \hat{f}_b) \end{bmatrix} \quad (5)$$

where $\boldsymbol{\rho}$ is the vehicle position, $\dot{\boldsymbol{\rho}}$ is the velocity, $\boldsymbol{n} = \begin{bmatrix} 0 \\ n \\ 0 \end{bmatrix}$, n is orbital angular rate,

$[\boldsymbol{n} \times] = \begin{bmatrix} 0 & 0 & -n \\ 0 & 0 & 0 \\ n & 0 & 0 \end{bmatrix}$, $\boldsymbol{K}(n) = \begin{bmatrix} 3n^2 & 0 & 0 \\ 0 & -n^2 & 0 \\ 0 & 0 & 0 \end{bmatrix}$, $\hat{\boldsymbol{f}}_b$ is the estimation of the accelerometer drift.

Similarly, the attitude prediction employs the attitude motion equations as

$$\dot{\boldsymbol{q}} = 0.5\boldsymbol{q} \otimes (\boldsymbol{\omega}_c - \hat{\boldsymbol{\omega}}_b - \boldsymbol{n}) \quad (6)$$

where \boldsymbol{q} is the vehicle attitude in quaternion form, \boldsymbol{C}_o^b is the corresponding rotation matrix, \boldsymbol{C}_b^o is the transpose matrix \boldsymbol{C}_o^b , That is $\boldsymbol{C}_b^o = \boldsymbol{C}_o^b{}^T$, $\hat{\boldsymbol{\omega}}_b$ is the estimation of the gyro drift.

The extravehicular vehicle's attitude, position and velocity parameters can be predicted by utilizing equations (5) and (6).

Because the structure and the shape of space stations is known, point cloud data which cover the surface of the space station can be generated. As the extravehicular vehicle drift over the target surface, point cloud data can be produced by employing a line laser triangulation measuring equipment. After match processing, relative position and relative attitude can be determined and denoted as $\boldsymbol{\rho}_c$ and \boldsymbol{q}_c respectively.

The relative pose produced by match processing does not diverge as working time pass by, but it can't provide velocity information and the time interval between measurements is too large to generate control instructions. Although prediction can produce all information and the output frequency is high, navigation error will become larger and larger as working time increasing. Therefore, a new integrated navigation system is proposed, and the system includes gyros, accelerometers and a line laser triangulation measuring equipment.

Equations (3) ~ (6) are selected as state equations, and $\boldsymbol{\rho}_c$ and \boldsymbol{q}_c are selected as measurements. State variables are defined as $[\boldsymbol{\rho}; \dot{\boldsymbol{\rho}}; \boldsymbol{q}; \boldsymbol{f}_b; \boldsymbol{\omega}_b]$, and then an extended Kalman filter(EKF) is adopted to estimate the states as,

Initialization:

$$\hat{\boldsymbol{X}}_0 = E[\boldsymbol{X}_0] \quad (7)$$

$$\boldsymbol{P}_0 = E[(\boldsymbol{X}_0 - E[\boldsymbol{X}_0])(\boldsymbol{X}_0 - E[\boldsymbol{X}_0])^T] \quad (8)$$

Time update:

$$\boldsymbol{X}_{k/k-1} = F(\boldsymbol{X}_{k-1}, \boldsymbol{w}_{k-1}) \quad (9)$$

$$\boldsymbol{P}_{k/k-1} = \boldsymbol{\Phi}_{k/k-1} \cdot \boldsymbol{P}_{k-1} \cdot \boldsymbol{\Phi}_{k/k-1}^T + \boldsymbol{Q}_{k-1} \quad (10)$$

Measurement update

$$\boldsymbol{K}_k = \boldsymbol{P}_{k/k-1} \cdot \boldsymbol{H}_k^T \cdot [\boldsymbol{H}_k \cdot \boldsymbol{P}_{k/k-1} \cdot \boldsymbol{H}_k^T + \boldsymbol{R}_k]^{-1} \quad (11)$$

$$\delta \hat{\boldsymbol{X}}_k = \boldsymbol{K}_k \cdot \boldsymbol{z}_k \quad (12)$$

$$\boldsymbol{P}_k = (\boldsymbol{I} - \boldsymbol{K}_k \cdot \boldsymbol{H}_k) \cdot \boldsymbol{P}_{k/k-1} \quad (13)$$

Therefore the estimated states $\boldsymbol{\rho}$, $\dot{\boldsymbol{\rho}}$, \boldsymbol{q} , \boldsymbol{f}_b and $\boldsymbol{\omega}_b$ can be innovated right after measurement update according to equations (9~13).

2.2 Point cloud data measurements and calibration

One of key technologies of this new integrated navigation system is point cloud data measurements. The measuring method should be low cost, small size, low power consumption and light weight. Therefore the line laser triangulation measuring has advantage, comparing with laser radar, binocular vision systems, etc. The line laser triangulation measuring equipment consists of an infrared laser, a camera and a filter sheet. The filter sheet is utilized to Shield visible light.

A laser beam irradiates at a certain angle on the target surface, and the laser is reflected. Because the incident and reflected light constitute a triangle, if the target objects moves along the direction of the laser beam, the laser beam image also move on the image plane corresponding. The target coordinates can be determined according to displacement relationship between the target the image. There are two line laser triangulation measuring system including direct and oblique type. Essentially the two are consistent, and then direct type is presented and discussed.

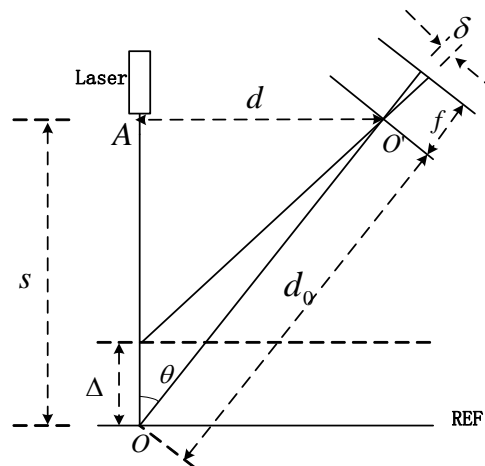


Fig. 2 Direct laser triangulation measurement

In Fig.2, s is distance between laser beam end A and datum plane REF. d_0 is the distance of OO' , f is the camera focal length, Δ is the distance between REF and target, δ is the corresponding image displacement, θ is the angle between laser beam and OO' . Then the measurement formula is derived as,

$$\Delta = \frac{d_0}{\frac{f \sin \theta}{\delta} + \cos \theta} \quad (7)$$

where d_0 , f and θ are constants and determined accurately before producing point cloud data. In reality, these parameters are difficult to be determined in designing. Therefore these parameters should be calibrated.

Because the laser beam end A is very difficult to be determined in reality, a new calibration method is proposed by using distance difference which avoids knowing laser beam end A . According to eq. (7), a new calibration model is presented as

$$y = \frac{1}{ax_{i+1} + b} - \frac{1}{ax_i + b} \quad (8)$$

where $y = \Delta_{i+1} - \Delta_i$, $x_{i+1} = 1/\delta_{i+1}$, $x_i = 1/\delta_i$, $a = f \sin \theta / d_0$, $b = \cos \theta / d_0$. According to eq. (8), it is obvious that it's a nonlinear model. y , x_{i+1} and x_i are known values, and a and b are to be estimated by calibration.

Gauss-Newton iterative method is employed to estimate a and b . After the number of iterations meets requirements or correction is less than a certain threshold value, the estimation of a and b is calculated. Because the focal length f can be determined by the camera calibration which are discussed by other papers, the θ and d_0 can be calculated as

$$\theta = \arctan(a/f \cdot b), \quad (9)$$

$$d_0 = \cos \theta / b \quad (10)$$

3. EXPERIMENTS AND ANALYSIS

An experimental system is constructed in the lab. The platform includes a line infrared laser whose center length is 850nm, a filter sheet and an industrial camera. The industrial camera is MV3000uc which is 1024×768, pixel size is 3.2um×3.2um. The system is mounted on a platform which is two degrees of freedom. The experimental system are shown in Fig. 3.



Fig. 3 The experimental system

This system calibration needs to collect a group of relative depth data. The first step is to take a common flat as a calibration flat placed just in front of the line laser, and keep calibration flat perpendicular to the laser beam direction. The second step is to move along the direction of laser beam several times, and the moving distances are 0cm, 5cm, 10cm, 15cm..., and the total movement 10 times. With the increase of the distance of the moving flat, the image position of the laser beam on the camera imaging plane is constantly moving, as shown in Fig. 4.

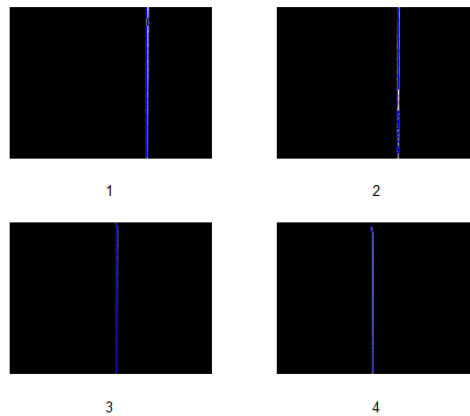


Fig. 4 Laser line moving process on camera imaging plane

After camera calibration, the focal length is 15.3mm. A group of images are processed, including image processing and calibration processing, $a=0.0052$, $b=0.0016$. Therefore the parameters of the experimental system are $\theta=12.04^\circ$, $d=128.32\text{mm}$, and distance s between laser beam end A and datum plane REF is 601.56mm.

In order to verify the calibration accuracy and analyze the point cloud data's quality. The distance difference is utilized to execute the evaluation. In this experiment, a calibration flat is moved once every 50mm and a set of images are collected. According to the obtained value δ after the image processing and the parameters of the measurement system, the distance between the laser beam end and the calibration flat is calculated by the eq. (7), which can be used to test whether the parameters are accurate. The experimental results are shown in Tab. 1.

Tab. 1 Point cloud data evaluation

| No. | 1 | 2 | 3 | 4 | 5 | 6 | 7 | 8 | 9 | 10 |
|-------------------|-------|-------|-------|-------|-------|-------|-------|-------|-------|-------|
| Distance(mm) | 431.0 | 477.5 | 526.5 | 578.5 | 628.5 | 679.8 | 732.2 | 782.9 | 831.4 | 878.9 |
| Displacement (mm) | - | 46.5 | 49.0 | 52.0 | 50.0 | 51.3 | 52.4 | 50.7 | 48.5 | 47.5 |

According to the data in the Tab. 1, in the range of 900mm to 400mm, the measurement error caused by a series factors is better than 4mm. The experimental data show that accuracy of the line laser triangulation measuring equipment proposed in this paper can reach millimeter level.

4. CONCLUSIONS

This paper proposed a new extravehicular vehicle to assist astronauts to inspect the surface of big spacecraft to guarantee safety of space activity. The

experiments shown that line laser triangulation measuring equipment proposed in this paper can reach millimeter level. The new integrated navigation system can be predicted to reach the high accuracy, and has advantages in scenario without GNSS signals.

REFERENCES

- M.L. Andrew, G. R. Matthew, E. H. Daniel. (2007) "On-orbit servicing: a new value proposition for satellite design and operation", *Journal of Spacecraft and Rockets*, 44(4) 964-976.
- J.X. Liang, O. Ma. (2011) "Angular velocity tracking for satellite rendezvous and docking", *Acta Astronautica*, 69 1019–1028.
- W.f. Xu, B. Liang, B. Li, Y.S. Xu. (2011) "A universal on-orbit servicing system used in the geostationary orbit", *Advances in Space Research*, 48 95-119.
- A. Ellery, J. Kreisel, B. Sommer. (2008) "The case for robotic on-orbit servicing of spacecraft: Space reliability is a myth", *Acta Astronautica*, 63 632–648.
- R.B. Friend, (2008) "Orbital express program summary and mission over-view", *Proc. SPIE* 695803.
- R.M. Pinson, R.T. Howard, A.F. Heaton. "Orbital express advanced video guidance sensor: ground testing, flight results and comparisons", In: *AIAA Guidance, Navigation, and Control Conference and Exhibit*, Honolulu, Hawaii, Aug 2008, pp. 1-12.
- K. Landzettel. "Ongoing Space Robotics Missions: TECSAS / DEOS", Available from < http://www.dlr.de/rm/en/desktopdefault.aspx/tabid-3825/5963_read-8759>.
- AERCam Sprint "https://en.wikipedia.org/wiki/AERCam_Sprint#Follow_on".
- Debus TJ, Dougherty SP. "Overview and performance of the front-end robotics enabling near-term demonstration (FRIEND) Robotic Arm", In: *AIAA Infotech@Aerospace Conference*. Seattle, WA, 6-9 April 2009, AIAA 2009-1870.
- Mini AERCam, "<http://aercam.jsc.nasa.gov/>".